Influence of pulse duration on mechanical effects after laser-induced breakdown in water

Joachim Noack[a)]
Medical Laser Center Lübeck GmbH, Peter-Monnik-Weg 4, D-23562 Lübeck, Germany

Daniel X. Hammer
Department of Biomedical Engineering, University of Texas, Austin, Texas 78712

Gary D. Noojin
TASC, 4241 Woodcock Drive, Suite B-100, San Antonio, Texas 78228

Benjamin A. Rockwell
Optical Radiation Division, Armstrong Laboratory, Brooks Air Force Base, Texas 78235

Alfred Vogel
Medical Laser Center Lübeck GmbH, Peter-Monnik-Weg 4, D-23562 Lübeck, Germany

(Received 10 December 1997; accepted for publication 10 March 1998)

The influence of the pulse duration on the mechanical effects following laser-induced breakdown in water was studied at pulse durations between 100 fs and 100 ns. Breakdown was generated by focusing laser pulses into a cuvette containing distilled water. The pulse energy corresponded to 6-times breakdown threshold energy. Plasma formation and shock wave emission were studied photographically. The plasma photographs show a strong influence of self-focusing on the plasma geometry for femtosecond pulses. Streak photographic recording of the shock propagation in the immediate vicinity of the breakdown region allowed the measurement of the near-field shock pressure. At the plasma rim, shock pressures between 3 and 9 GPa were observed for most pulse durations. The shock pressure rapidly decays proportionally to $r^{-(2\cdots3)}$ with increasing distance r from the optical axis. At a 6 mm distance of the shock pressure has dropped to (8.5 ± 0.6) MPa for 76 ns and to <0.1 MPa for femtosecond pulses. The radius of the cavitation bubble is reduced from 2.5 mm (76 ns pulses) to less than 50 μm for femtosecond pulses. Mechanical effects such as shock wave emission and cavitation bubble expansion are greatly reduced for shorter laser pulses, because the energy required to produce breakdown decreases with decreasing pulse duration, and because a larger fraction of energy is required to overcome the heat of vaporization with femtosecond pulses.
 [S0021-8979(98)00312-0]

I. INTRODUCTION

When high intensity laser pulses are focused into a transparent medium, such as water, they can produce a plasma in the medium through multiphoton and cascade ionization.[1–3] This plasma formation is called laser-induced breakdown and has been observed in solids,[2,4] liquids,[2,5,6] and gases.[7] In solids, laser-induced breakdown not only leads to material damage in the breakdown region itself, but also causes micro-cracks if the pressure exerted by the plasma on the surrounding material exceeds the dynamic yield strength.[2,4] The sudden pressure rise in the breakdown region also leads to an emission of a shock wave into the surrounding medium, which might cause additional damage.

Laser-induced breakdown in liquids is mainly of interest for medical laser applications, such as intraocular photodisruption,[8,9] where it is used for the evaporation of transparent tissues. In liquids, laser-induced breakdown not only leads to shock wave emission, but also to the creation of a cavitation bubble which contains the evaporated material.[2,5,10] This vapor bubble first expands and then collapses under the hydrostatic pressure.[11]

The gross tissue displacement and tearing caused by the cavitation bubble oscillation has been identified as a major source of collateral damage in nanosecond photodisruption.[12,13] Even though the shock wave does not cause morphological damage, in vitro experiments revealed that the shock wave changes the cell membrane permeability,[15] influences cell viability,[15,16] and can cause fracturing of deoxyribonucleic acid (DNA) strands.[16]

It has been shown that mechanical effects and therefore unwanted side effects associated with laser-induced breakdown are significantly reduced, if shorter laser pulses are used,[12,17–19] mainly because the pulse energy required to produce optical breakdown decreases with decreasing pulse duration.[6,20,21] In this paper, the influence of the pulse duration on the mechanical effects was studied in order to create a framework for an optimization of laser parameters for intraocular photodisruption and related applications.

II. EXPERIMENTAL METHODS

A. Creation of laser-induced breakdown

Laser-induced breakdown was created by focusing laser pulses with different durations into a cuvette containing high

a)Electronic mail: noack@mll.mu_luebeck.de

TABLE I. Experimental parameters.

Pulse duration	Wavelength (nm)	θ (deg)	Energy ($E_{in}/\mu J$)	Transmission (%)
76 ns	750	19	33 000.0	4 ± 1
6 ns	1064	22	730.8	7 ± 1
60 ps	532	13	24.6	52 ± 3
3 ps	580	16	3.1	77 ± 2
300 fs	580	16	1.7	59 ± 10
100 fs	580	16	1.0	49 ± 2

purity distilled water. The laser pulses were generated by an Alexandrite laser ($\tau_L = 76$ ns, Light-Age Inc.), a Nd:YAG laser ($\tau_L = 6$ ns, Continuum YG 671-10), and a dye-laser system ($\tau_L = 3$ ps, 300 fs, 100 fs, Spectra-Physics). A pulse energy corresponding to a sixfold breakdown threshold was used in all experiments. The experimental parameters are summarized in Table I.

The setup for the generation and observation of laser-induced breakdown is depicted in Fig. 1. The laser beam was expanded using a biconcave lens ($f_1 = -20 - -40$) followed by a laser achromat ($f_2 = 200$ mm). The expanded beam with a diameter of 19–26 mm was focused into the sample by another achromat ($f_3 = 120$ mm) and an ophthalmic contact lens (f_4, Rodenstock RYM) built directly into the wall of the cuvette. The contact lens minimized spherical aberrations at the laser focus. For 76 ns pulses the risk of mechanical damage to the contact lens was very high, and it was therefore replaced by a plano-convex lens ($f_4 = 100$ mm in air), resulting in increased spherical aberrations and a larger spot size. The measured far-field focusing angles θ determined by knife-edge measurements[22] are listed in Table I.

The energy delivered into the cuvette as well as the energy transmitted within the focusing angle were measured by calibrated pyroelectric detectors ($ED_{1,2}$). The pulse energies used as well as the measured transmission values are summarized in Table I. A detailed discussion of the breakdown thresholds and the transmission can be found in Ref. 23.

B. Observation of events

A two stage imaging system was employed to monitor the events in the cuvette by simultaneous streak and framing photography. The first stage (L_5, EL Nikkor 63 mm, $F = 4$) imaged the breakdown region onto a glass substrate with a highly reflecting coating placed under 45° with respect to the optical axis. The coating had a 20 μm wide uncoated slit and the transmitted part of the image was reimaged by a second lens (L_6, Nikon 105/5.6) onto the photocathode of a streak camera. The image reflected at the glass substrate was imaged onto a camera back by another lens (L_7). The magnification from object to film varied between 11× and 45× for the framing images and between 16× and 71× for the streak images. The large magnification was used for the events created by the ultrashort laser pulses with low pulse energy.

The streak images were back-illuminated by pulses from a flashlamp pumped dye laser ($\lambda = 630$ nm) coupled to a few meters of 300 μm optical fiber (L_{10}). The exit fiber tip was imaged into the object volume by lens L_{11} to provide a homogeneous illumination with 200–500 ns duration. The framing photographs, in contrast, were illuminated by another dye laser emitting subnanosecond pulses. In the 6 ns experiments, a small fraction of the laser pulse generating the breakdown event was frequency-doubled and used for illumination instead. The delay between the generation of the breakdown event and the framing image was adjusted either electronically or optically. The two illuminating beams were combined in front of the cuvette using a dichroic mirror (DM) and separated by suitable band pass (BP, $\lambda = 630 \pm 5$ nm) and short pass (SP, $\lambda > 600$ nm) filters.

In addition to the photographic investigations, the shock wave pressure was measured several millimeters away from the breakdown site using a factory calibrated hydrophone (Ceram) with an active area of 1 mm^2 and a rise time of 12 ns.

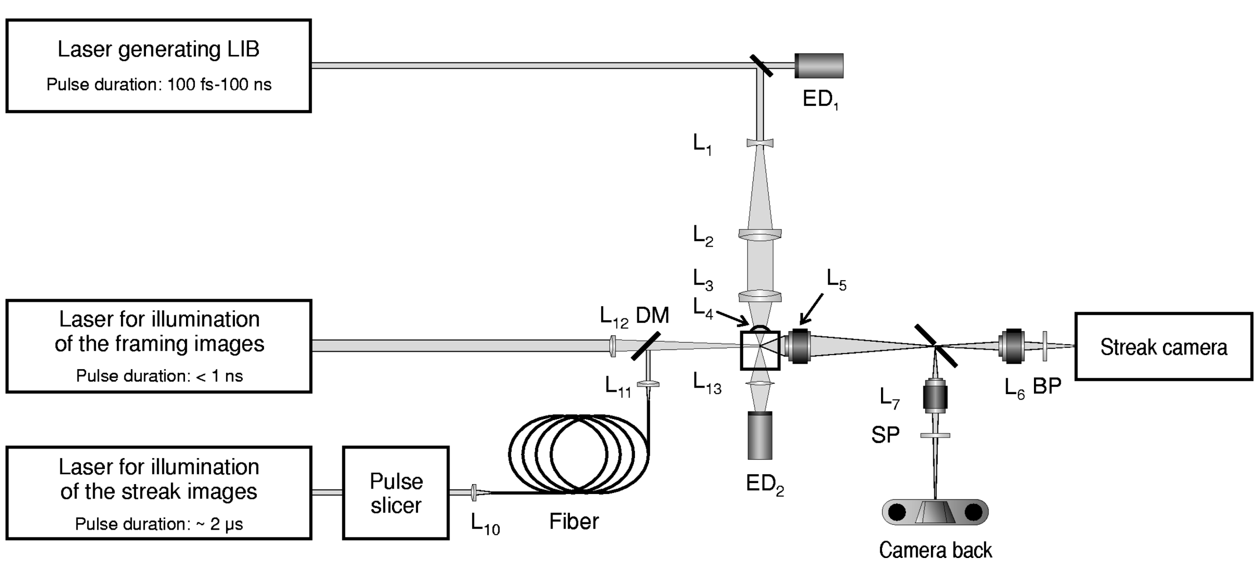

FIG. 1. Experimental setup for simultaneous streak and framing photography.

C. Data analysis

The near-field shock pressure was obtained from the streak images. For this purpose the position $r(t)$ of the shock wave was extracted from the streak images as a function of time t using image processing techniques.[23,24] Differentiation of the $r(t)$ curves yielded the shock wave velocity u, which is related to the shock peak pressure p by[10,24]

$$p=A\rho_0 u(10^{(u-c_0)/B}-1), \tag{1}$$

where $c_0=1483\ \mathrm{ms}^{-1}$ and $\rho_0=998\ \mathrm{kg\ m}^{-3}$ denote the sonic velocity and the density of the undisturbed water. $A=5190\ \mathrm{ms}^{-1}$ and $B=25306\ \mathrm{ms}^{-1}$ are empirical constants determined from Rankine–Hugoniot data.[25]

The hydrophone measurements not only yielded the far-field shock pressure, but were also used to determine the maximum radius $R_{\max}$ of the cavitation bubble, which is related to the cavitation bubble oscillation period $2T_c$ by Rayleigh's formula[26]

$$R_{\max}=\frac{T_c}{0.915\sqrt{\dfrac{\rho_0}{p_0-p_v}}}. \tag{2}$$

p_v denotes the vapor pressure at ambient temperature and p_0 is the atmospheric pressure. The oscillation period is indicated by the time between the shock waves from breakdown and bubble collapse. The mechanical energy E_B of a spherical cavitation bubble is then given by[10]

$$E_B=\tfrac{4}{3}\pi(p_0-p_v)R_{\max}^3. \tag{3}$$

III. RESULTS

A. Plasma

Figure 2 shows the appearance of the breakdown region for laser pulses with six different pulse durations. The images obtained after nanosecond breakdown show a luminescent plasma surrounded by a cavitation bubble and an outward propagating shock wave [Figs. 2(a) and 2(b)]. A luminescent plasma was also observed for 60 ps pulses, but was too weak to be detected on the film at 42×. For even shorter laser pulses no plasma radiation could be observed at all.

Since the images were obtained with an open shutter in a dark room, any plasma luminescence was imaged regardless of the delay between the breakdown and the illumination pulse. For 6 ns pulses, for example, the plasma luminescence lasted only for ~15 ns and had therefore already ceased when the shock wave and cavitation bubble in Fig. 2(b) were photographed. If any significant expansion takes place during the lifetime of the luminescent plasma, the time-integrated photographs show the plasma dimensions up to the point where the plasma emission becomes too weak to expose the film, i.e., the image of the luminescent plasma is larger than the actual breakdown region. This is particularly true for the 76 ns pulses where plasma radiation was observed for more than 200 ns.

The shape of the breakdown region indicated by the form of the luminescent plasma (nanosecond pulses) and the form of the initial cavitation bubble (for the other pulse durations) changes from conical to cylindrical with decreasing pulse duration [Figs. 2(a)–2(f)]. For femtosecond pulses two separate breakdown sites [Fig. 2(e)] and inhomogeneities in their appearance [Fig. 2(f)] were observed.

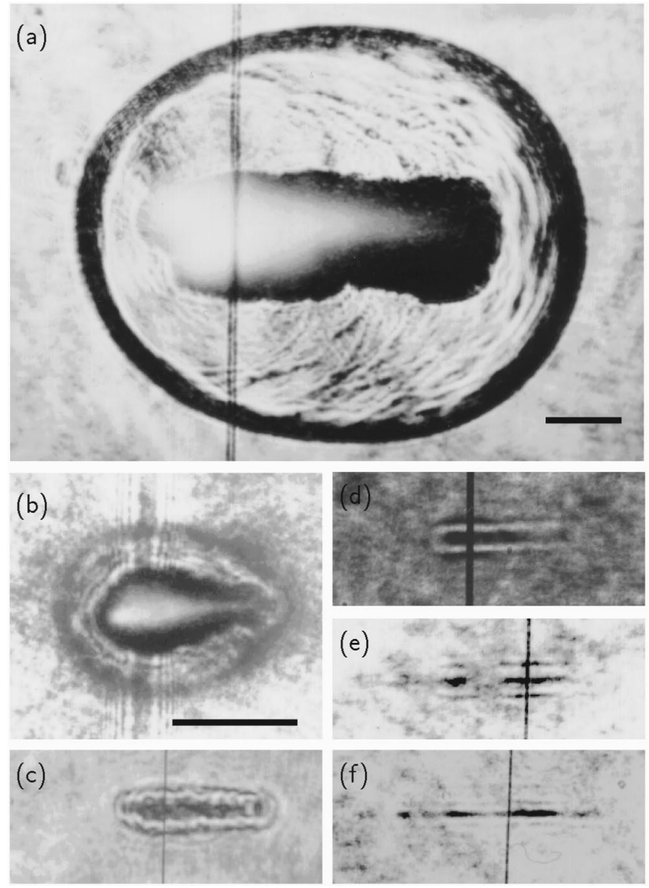

FIG. 2. Laser-induced breakdown with laser pulses of different durations: (a) 76 ns, (b) 6 ns, (c) 60 ps, (d) 3 ps, (e) 300 fs, and (f) 100 fs. The images were illuminated with a dye laser pulse 120 ns (76 ns pulses), 23 ns (6 ns pulses), and 3 ns (others) after the creation of breakdown. The laser pulses incident from the left had an energy corresponding to 6-times the breakdown threshold. The length of the scale is 100 μm in (a) and (b); images (b)–(f) are of equal magnification. The vertical lines indicate the position of the streak slit.

B. Shock wave

Streak images of the shock wave emission following laser-induced breakdown are shown in Fig. 3. Because the plasma radiation was blocked by a band pass filter (BP, Fig. 1), the plasma appears as a dark object in the streak images when optical breakdown occurs (right). As time progresses, the plasma starts to form the cavitation bubble which becomes the central dark object in the images. The two inclined dark lines above and below correspond to the shock wave propagating outward. For 100 fs pulses, no useable streak image of the shock wave could be obtained due to poor contrast of the shock wave.

The slope of the shock trajectory, corresponding to the shock wave velocity, gradually decreases with time (i.e., from left to right), soon approaching the sonic velocity c_0. Whereas with 76 ns pulses a supersonic velocity was ob-

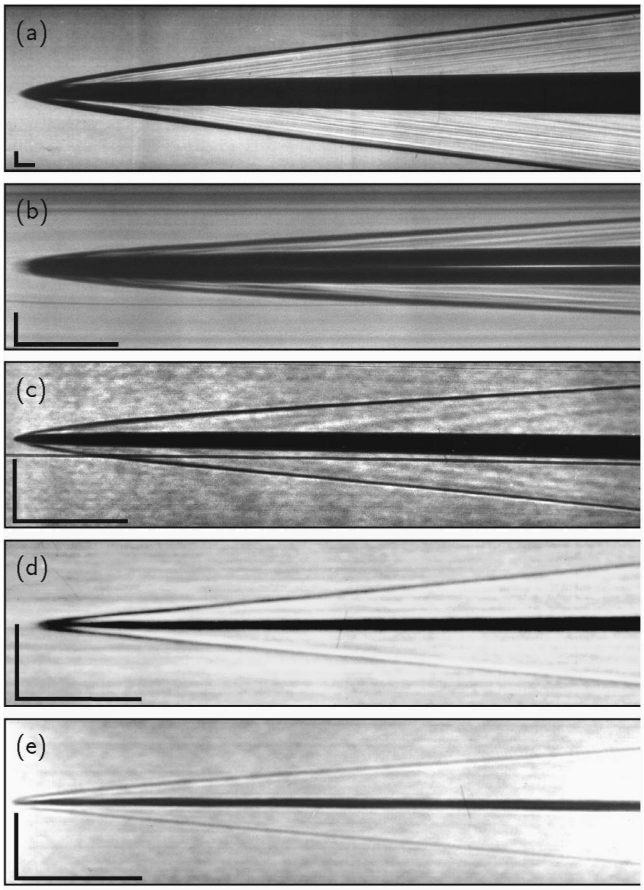

FIG. 3. Streak images of shock wave emission after laser-induced breakdown with laser pulses of (a) 76 ns, (b) 6 ns, (c) 60 ps, (d) 3 ps, and (e) 300 fs duration. The length of the bars represents 10 ns (horizontally) and 100 μm (vertically).

served during the first 160 ns, the shock speed observed after 3 ps and 300 fs breakdown differed from the sonic velocity only during the first 10 ns.

The shock wave speeds extracted from the streak images using digital image processing[23,24] were converted to shock pressures using Eq. (1), and are plotted in Fig. 4 as a function of distance from the optical axis. When the shock wave detaches from the cavitation bubble the shock pressure was found to be between 3 and 9 GPa. Only for 3 ps pulses was a substantially lower shock pressure of 0.3 GPa found.

The shock wave pressure decays rapidly below 0.1 GPa, where the deviation of the propagation velocity from sonic velocity becomes too small to be measured accurately with the streak technique.[23,24] The pressure decay is approximately proportional to r^{-3} for 6 ns, 60 ps, and 300 fs pulses. For 76 ns pulses a pressure decay proportional to $r^{-2.2}$ was observed. The pressure decay ($\propto r^{-1.3}$) observed with 3 ps pulses has to be interpreted with great care because of the large uncertainty (87%) at pressures on the order of 0.1 GPa.[23,24]

The shock wave width cannot be inferred from the streak images. The shock trajectories are visualized, because the refractive index gradient induced by the shock wave refracts the illumination light out of the imaging aperture. The width of the shock wave image is therefore determined by the pressure profile, the pressure amplitude, and the aperture of the imaging lens. Thus the width of shock trajectory should not be mistaken for the shock width.

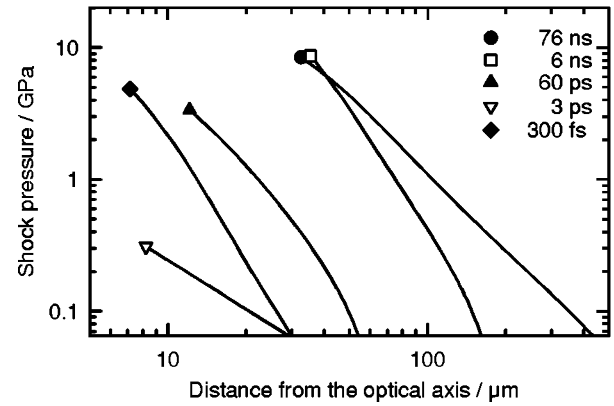

FIG. 4. Shock wave pressure as a function of distance from the optical axis for different pulse durations. Each curve represents a single event. The location of each symbol indicates the point where the shock wave detaches from the cavitation bubble or plasma.

The shock wave profiles measured a few millimeters away from the breakdown site using a fast hydrophone are shown in Fig. 5. The hydrophone signals generated by nanosecond breakdown show a fast rise followed by a slower decay. The full width half maximum (FWHM) of the signals is 120 and 80 ns for 76 and 6 ns pulses, respectively. The width of the signals observed after breakdown with pico- and femtosecond pulses was $\approx$25 ns regardless of the pulse duration. In these cases the signal is limited by the temporal resolution of the hydrophone used.

The far-field pressure at a distance of 6 mm decreases by 2 orders of magnitude from 8.5 MPa for 76 ns pulses to 60 kPa for femtosecond pulses (Table II). To avoid damage to the pressure transducer, pressure measurements for 76 ns pulses were performed in the range $r = 10-17.5$ mm and extrapolated to 6 mm assuming $p \propto 1/r$.

C. Cavitation bubble

The period of the first cavitation bubble oscillation and the maximum bubble radius predicted by Eq. (2) are also

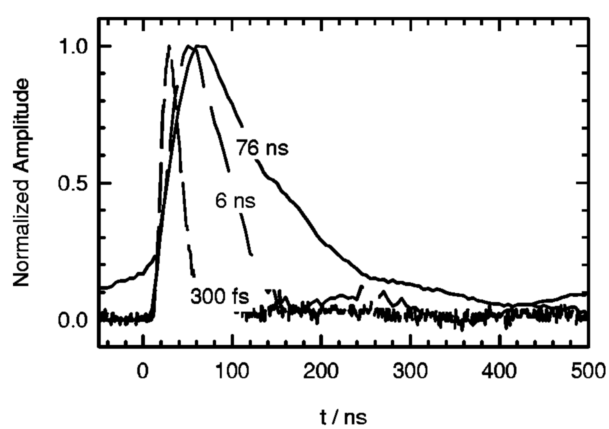

FIG. 5. Normalized hydrophone signals observed in the far-field after laser-induced breakdown with different pulse durations. The hydrophone signals were obtained at 10 mm (76 ns), 9 mm (6 ns), and 6 mm (300 fs) from the breakdown site.

TABLE II. Shock wave pressures at 6 mm distance and parameters of the cavitation bubble.

Pulse duration (τ_L)	Shock pressure (p/MPa)	Period ($2T_c/\mu$s)	Bubble radius (R_{max}/μm)	Conversion (η_{dep}/%)
76 ns	8.50±0.6[a]	468.0±7.4	2560±41	21.6±1.6
6 ns	1.97±0.20	126.1±9.2	690±50	19.8±3.3
60 ps	0.27±0.04	25.4±1.8	139±10	8.6±2.0
3 ps	0.11±0.01	12.8±0.6	70±3	9.0±2.1
300 fs	0.07±0.01	10.4±0.8	57±4	9.3±2.4
100 fs	0.06±0.01	8.0±0.8	44±4	6.5±2.1

[a]Extrapolated from $p=5.5\pm0.4$ MPa at 10 mm.

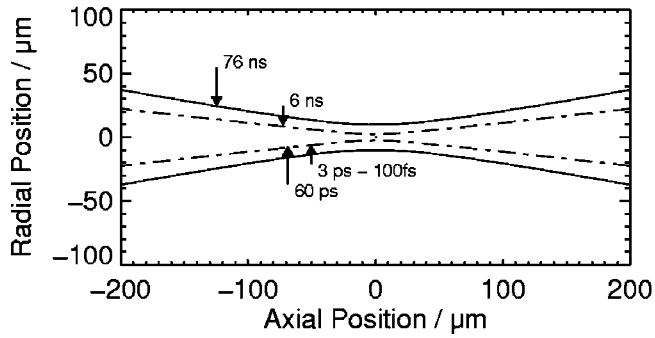

FIG. 6. Geometry of the beam waist ($1/e^2$ contours). The axial position of the arrow indicates the plasma length predicted by the moving breakdown model for pulse energies of six times threshold.

listed in Table II. The radius of the expanded cavitation bubble decreases from 2.5 mm for 76 ns pulses to less than 50 μm for 100 fs pulses. It might be assumed that the reduced size is caused only by the smaller amount of energy deposited into the focal volume for shorter pulses, therefore the conversion efficiency

$$\eta_{dep}=E_B/(1-T)E_{in} \tag{4}$$

from deposited energy into cavitation bubble energy is also given in Table II. Whereas for nanosecond pulses around one fifth of the deposited laser pulse energy contributes to the creation of the cavitation bubble, only 6.5% of the pulse energy is converted to mechanical energy of the cavitation bubble created by 100 fs pulses.

IV. DISCUSSION

A. Plasma

The threshold for laser-induced breakdown is an intensity threshold,[6,27,28] therefore breakdown should occur along isointensity lines[27,29] with $I=I_{th}$. At threshold energy E_{th} breakdown occurs where maximum light intensity is encountered, i.e., in the beam waist $(z=0)$. With increasing pulse energy, the critical intensity is also exceeded at larger cross sections along the beam path and a larger plasma length results. Plasma growth preferentially takes place towards the laser because most of the energy is absorbed by the plasma generated before the beam waist.[6,30] This is particularly true for nanosecond pulses, where only a few percent of the incident energy is transmitted through the focal region.

Figure 6 shows the $1/e^2$ contours for the 76 ns and the 3 ps experiments measured by a knife-edge technique.[22] The beam waist for the other pulse durations was almost identical to the 3 ps curve and is thus omitted for clarity. At six times threshold energy, the plasma should extend from the focus, up to the point (arrows) where the beam cross section is six times larger than in the beam waist. The geometry of the beam waist and the predicted plasma length can be directly compared to the shape of the plasmas in Figs. 2(b)–2(f) which are enlarged to the same scale.

Discrepancies between experiment and prediction exist in shape and size: The plasmas observed with nanosecond pulses are always larger than expected. This difference is most pronounced for the 76 ns pulses where the observed plasma length of 400 μm is more than twice as large as predicted. For 6 ns pulses the length of the plasma is 1.6 times longer than expected. In both cases, however, the observed conical shape is consistent with the beam geometry. This is in contrast to the 100 fs pulses, where the cylindrical plasma shape is inconsistent with the large plasma length observed.

There are two factors that lead to the long plasmas length observed with nanosecond pulses: First of all there might have been a plasma expansion during the luminescence lifetime of the plasma which leads to an overestimation of the plasma length in the framing photographs. The overestimation will be most pronounced for the 76 ns pulses because of the long plasma luminescence. Figure 3(a) indicates, however, that the radial growth of the cavitation bubble after the end of the laser pulse is slow and this is also true for the axial growth (unpublished data). It seems therefore unlikely that plasma expansion is the only factor contributing to the long plasma length. Another possible mechanism is the interaction between the plasma radiation and the surrounding medium.[6] The breakdown threshold for nanosecond pulses in pure water is given by the intensity required for the production of the first free electrons by multiphoton absorption.[6,21,28] Subsequently, these initial electrons are rapidly multiplied by cascade ionization, resulting in a luminescent plasma. In the vicinity of a plasma, free electrons can also be produced by absorption of ultraviolet (UV) radiation emitted by the plasma. In this case, multiphoton absorption as a source of seed electrons is no longer required and the breakdown threshold I_{th} drops during the laser pulse,[6] thus explaining the longer plasma length.

The low transmission (Table I) through the plasma indicates that plasma growth beyond the beam waist $(z>0)$ can be neglected for nanosecond pulses. For picosecond pulses, however, more than half of the incident energy reaches the region beyond the focus and might therefore lead to plasma formation in this region. For 3 ps pulses, a total plasma length of 90 μm was observed, whereas according to the measured beam profile the plasma should extend 50 μm from the waist towards the laser. Considering the fact that only 23% of the pulse energy is absorbed in the breakdown region it does not seem unlikely that the plasma length extends beyond the waist almost equaling the plasma length before the focus, thus explaining the measured plasma length. The plasma transmission at 60 ps is lower than for

3 ps pulses and therefore a larger fraction of the total plasma length (110 μm) appears before the beam waist (70 μm).

The plasma shape observed with femtosecond pulses can neither be explained by a changing breakdown threshold during the laser pulse, nor by changes in plasma transmission. If similar to longer pulse durations, the shape of the breakdown region is indicative of the intensity distribution, the narrow plasma filaments suggest that the initially Gaussian intensity distribution must have changed significantly during propagation due to self-focusing. The critical power P_{cr} for self-focusing at 580 nm is given by[31,32]

$$P_{cr}=3.77\frac{c\lambda^2}{32\pi^2 n_2}\approx 1\ \text{MW}. \tag{5}$$

This is significantly lower than the peak power in the experiments, which was 5.6 and 17 MW for 300 and 100 fs pulses, respectively. Thus self-focusing is expected to occur for femtosecond laser pulses.[33]

B. Shock wave

1. Plasma rim

The location of the plasma rim for pico- and femtosecond pulses can be determined with reasonable accuracy from the framing images in Fig. 2. Due to the expansion of the 76 ns plasmas during their radiant lifetime this method leads to an overestimation of the radius where the shock wave detaches from the plasma, thus resulting in an underestimation of the shock pressure at the plasma rim. Therefore we have determined the plasma radius when the shock wave detaches from the cavitation bubble in the streak image (Fig. 3).

Despite the uncertainties in determining the plasma rim, the shock pressures observed with nanosecond pulses (8.5 GPa) are about twice as large as those observed with the other pulse durations, which is consistent with the observation of bright luminescent plasmas. The shock pressures observed with 60 ps and 300 fs pulses do not differ significantly (3–5 GPa). Only with 3 ps pulses significantly lower shock pressures (<1 GPa) were observed.

It is remarkable that, at six times threshold, the shock pressure closely follows the trends observed in transmission: For nanosecond pulses almost the entire pulse energy is deposited and thus the energy density of the plasmas created is very large, resulting in high shock pressures. The increasing transmission leads to a drastic reduction in energy density with decreasing laser pulse duration, and thus to a reduction of the shock pressures at the plasma rim at 3 ps. The increasing role of multiphoton absorption for subpicosecond pulses[23] leads to a transmission of 300 fs plasmas which is similar to those observed with 60 ps pulses, thus shock pressures are also similar.

2. Pressure decay

For all pulse durations, the shock pressure decreases faster with increasing propagation distance than in the acoustic limit, where a pressure decay proportional $1/r$ would be expected for a spherical source.[34] The fast pressure decay is caused by the energy dissipation at the shock front and the nonlinearity of propagation, which results in a modification of the pressure profile during propagation.[34,35] The fact that the speed of propagation increases with increasing pressure, causes the trailing edge of a shock wave to propagate significantly slower than the leading edge, resulting in shock wave broadening. This shock wave broadening is most pronounced in high pressure regions, i.e., near the source.[35] Based on the conservation of momentum, a $1/r^2$ dependence of the shock pressure can be derived[36] if shock wave broadening is negligible. This relationship is in reasonable accord with experimental data obtained with nanosecond and picosecond pulses at distances above 100 μm.[36]

Considering the shock wave broadening near the source, the finding of a pressure decay faster than r^{-2} in the immediate vicinity of the plasma for all pulse durations except 3 ps and 76 ns is not unexpected (Fig. 4). The significantly slower pressure decay for 76 ns may be caused by the fact that the high shock pressure is maintained by the continuing energy deposition during the rest of the laser pulse. The very slow pressure decay ($\propto r^{-1.3}$) observed for 3 ps pulses is not easy to understand. It may be an artefact because at 0.1 GPa the shock velocity deviates only by 9% from the sonic velocity. Such small variations from the sonic velocity are hardly detectable with the streak technique, resulting in a large measurement uncertainty.[23,24]

3. Far-field pressure

The shock pressure at a fixed distance from the optical axis decreases with decreasing pulse duration. This trend is observed in the far-field (Table II) as well as in the near-field (Fig. 4, except 3 ps), even though the shock pressures at the plasma rim are similar for most pulse durations. The main reason for the decreasing shock pressure is that the total energy deposited in the breakdown region decreases with decreasing pulse duration,[6,17,21] thus less energy is available for the generation of the shock wave and therefore the shock amplitude is reduced for shorter pulse durations.

The similarity law[35] states that the shock pressure at a distance r from the source with radius r_0 depends only on the ratio r/r_0. Since the plasma radius r_0 decreases with decreasing laser pulse durations (Fig. 2) the relative distance r/r_0 increases for $r=$const. Thus a decreasing shock pressure at a fixed distance r is expected for shorter laser pulses, even if the energy density in the plasma was independent of the pulse duration.

The far field shock pressures for pico- and femtosecond pulses are similar to those reported by Hammer *et al.*[17] closer to the source (1 mm), where higher shock pressures are to be expected. This apparent discrepancy could be caused by the slower hydrophone used in the previous study (risetime 30 ns), which does not record the correct pressure amplitude, if the shock wave duration is significantly shorter than the rise time.[37] The results for 60 ps and 6 ns pulses are in reasonable accord with pressures observed in 10 mm distance from breakdown with 30 ps pulses at ten times threshold (0.24 MPa) and 6 ns pulses at eight times threshold (0.99 MPa).[10]

4. Shock wave width

Considering the explosive behavior of the electron cascade during nanosecond breakdown[23] it is reasonable to assume an almost instantaneous pressure rise in the breakdown region during the initial phase of the laser pulse. Thus a high pressure shock wave starts to propagate into the surrounding medium. With time the breakdown region starts to expand and the pressure inside the plasma (initial cavitation bubble) decreases. If the energy deposition is almost instantaneous, i.e., no energy deposition takes place during the expansion of the cavitation bubble, the width of the shock wave is only determined by the speed of cavitation bubble expansion. If, however, the high pressure inside the plasma is maintained during the expansion by further energy deposition, the duration of the high pressure transient will be prolonged. Therefore the shock waves created by breakdown with 76 ns pulses have a larger width than those created by shorter laser pulses (Fig. 5). The duration is also longer, because the width of a shock wave emitted from a source with radius r_0 (and a given energy density) increases proportional to the radius,[35] and the radius of a 76 ns plasma is much larger than of a 6 ns plasma (Fig. 2).

The shock pressures as well as the shock width observed with pico- and femtosecond pulses in the far-field have to be interpreted with great care, because of the detector bandwidth. The true shock width may be smaller than the width of the signals in Fig. 5. For femtosecond pulses, a lower limit for the shock width is given by the time for the shock wave to transverse the plasma in radial direction, i.e., the minimum possible shock wave width is on the order of 2–3 ns. However, it's actual duration is determined by the bubble expansion. The fact that the geometry of the plasma is similar for pulse durations of 3 ps and less, suggests that the initial cavitation bubble dynamics and thus the shock width is comparable for pulse durations between 100 fs and 3 ps. For 3 ps pulses the shock waves might be slightly longer because of the low energy density in the plasma, which could result in a slower cavitation bubble expansion.

C. Cavitation bubble

The size and thus the energy coupled into the cavitation bubble decreases with decreasing pulse duration because:

(1) the pulse energy required to produce breakdown decreases with the decrease in pulse duration;[6,21]
(2) a larger percentage of the pulse energy is transmitted for shorter pulse durations (Table I, with an inversion of the trend for subpicosecond pulses); and
(3) a larger fraction of the pulse energy is required to evaporate the focal volume for shorter pulses and thus less energy is available for mechanical processes.

The volume of the breakdown region can be estimated from the plasma photographs in Fig. 2. This, in combination with the transmission measurements, allows a rough estimate of the energy density within the breakdown region. Whereas the energy density for nanosecond pulses ($\approx$40 kJ/g, Ref. 10) is well in excess of the enthalphy of evaporation which is 2.3 kJ/g for water, it is less than 0.6 kJ/g for femtosecond pulses. Thus complete evaporation of the breakdown volume is possible for nanosecond pulses, but only part of the breakdown region can be evaporated by femtosecond pulses.

The conversion from light to bubble energy for 3 ps and femtosecond pulses is similar (Table II), despite the fact that a larger fraction of the pulse energy is transmitted with 3 ps pulses (Table I). This indicates that for femtosecond pulses, a larger fraction of the deposited energy does not contribute to the bubble formation. This is due to the inhomogeneities arising through self-focusing, where a region of low energy density is formed around a filament with high energy density.[38,39] The inhomogeneity of the energy density is also an explanation of why a cavitation bubble is formed although the average energy density in the breakdown region is below the evaporation enthalpy.

Cavitation bubble sizes (Table II) agree well with previously published data for pulse energies around ten times threshold. Reported values for 100–400 fs pulses are 40–50 μm,[17,41] 80 μm for 3 ps pulses,[17] 150–255 μm for pulse durations between 20 and 60 ps,[10,17,40] and 800 μm for 6 ns.[10] The small discrepancies to the values listed in Table II can be explained by the slightly different pulse energies and focusing geometries.

It has been pointed out earlier[17] that the cavitation bubbles created by femtosecond pulses remain aspherical throughout their entire lifetime. This asphericity is caused by the fact that the cavitation bubble energy becomes so small that the lateral expansion is less than the plasma length (which is enlarged under the influence of self-focusing).

V. CONCLUSIONS

Mechanical effects such as cavitation and shock wave emission are reduced significantly for shorter laser pulse durations, mainly because the threshold energy and thus the energy available for mechanical effects decreases for shorter laser pulses. Additionally, the partition of the incident pulse energy into transmitted energy, cavitation bubble energy, shock wave energy, and heat of vaporization changes with decreasing pulse duration. Whereas for nanosecond pulses most of the incident pulse energy is coupled into mechanical effects,[10] the transmitted energy and the heat of vaporization are the most important energy channels for femtosecond pulses.

For ophthalmic laser applications, the reduced size of the cavitation bubble implies less tissue displacement and tearing. The damage potential of shock waves is also reduced, because at a given distance shock pressures are lower for femtosecond pulses. Femtosecond pulses might therefore offer an increased surgical precision over current techniques. If, however, disintegration of a larger tissue volume is required to produce a therapeutic effect, a large number of femtosecond pulses should be applied instead of increasing the pulse energy due to the strong role of self-focusing. To avoid interaction of the following laser pulses with the cavitation bubble or residual gas bubbles created by earlier pulses[41,42] the repetition rate should be limited to a few kilohertz. Due to the high transmission, pulse durations around 1 ps[23] are particularly unsuited for opthalmic laser applications, because the transmitted light poses an unnecessary risk to the retina.

ACKNOWLEDGMENTS

This work has been supported by the German Research Foundation and the Air Force Armstrong Laboratory, Air Force Material Command, Brooks Air Force Base, Texas.

[1] P. K. Kennedy, D. X. Hammer, and B. A. Rockwell, Prog. Quantum Electron. **21**, 155 (1997).
[2] J. F. Ready, *Effects of High-Power Laser Radiation* (Academic, London, 1971).
[3] Y. R. Shen, *The Principles of Nonlinear Optics* (Wiley, New York, 1984), Chap. 27.
[4] W. Koechner, *Solid State Laser Engineering* (Springer, Berlin, 1988), and references therein.
[5] M. P. Felix and A. T. Ellis, Appl. Phys. Lett. **19**, 484 (1971).
[6] A. Vogel, K. Nahen, D. Theisen, and J. Noack, IEEE J. Sel. Top. Quantum Electron. **2**, 847 (1996).
[7] C. DeMichelis, IEEE J. Quantum Electron. **QE-5**, 188 (1969).
[8] D. Aron-Rosa, J. Aron, J. Griesemann, and R. Thyzel, Am. Intra-Ocul. Implant Soc. J. **6**, 352 (1980).
[9] A. Vogel, Phys. Med. Biol. **42**, 895 (1997).
[10] A. Vogel, S. Busch, and U. Parlitz, J. Acoust. Soc. Am. **100**, 148 (1996).
[11] A. Vogel, W. Lauterborn, and R. Timm, J. Fluid Mech. **206**, 299 (1989).
[12] A. Vogel, S. Busch, K. Jungnickel, and R. Birngruber, Lasers Surg. Med. **15**, 32 (1994).
[13] A. Vogel, M. R. C. Capon, M. N. Asiyo-Vogel, and R. Birngruber, Invest. Ophthalmol. Visual Sci. **35**, 3032 (1994).
[14] A. Vogel, P. Schweiger, A. Frieser, M. N. Asiyo, and R. Birngruber, IEEE J. Quantum Electron. **26**, 2240 (1990).
[15] A. G. Doukas and T. J. Flotte, Ultrasound Med. Biol. **22**, 151 (1996).
[16] K. Teshima, T. Ohshima, S. Tanaka, and T. Nagai, Shock Waves **4**, 293 (1995).
[17] D. X. Hammer, R. J. Thomas, M. Frenz, E. D. Jansen, G. D. Noojin, S. J. Diggs, J. Noack, A. Vogel, and B. A. Rockwell, in *Laser Tissue Interaction VII*, Proc. SPIE edited by S. L. Jacques (SPIE, Bellingham, WA, 1996), Vol. **2681A, pp.** 437–448.
[18] T. Juhasz, X. H. Hu, L. Turi, and Z. Bor, Lasers Surg. Med. **15**, 91 (1994).
[19] T. Juhsaz, G. Kastis, C. Súarez, Z. Bor, and W. E. Bron, Lasers Surg. Med. **19**, 23 (1996).
[20] D. X. Hammer, R. J. Thomas, G. D. Noojin, B. A. Rockwell, P. K. Kennedy, and W. P. Roach, IEEE J. Quantum Electron. **QE-32**, 670 (1996).
[21] P. K. Kennedy, S. A. Boppart, D. X. Hammer, B. A. Rockwell, G. D. Noojin, and W. P. Roach, IEEE J. Quantum Electron. **31**, 2250 (1995).
[22] A. E. Siegman, M. W. Sasnett, and T. F. Johnston, IEEE J. Quantum Electron. **27**, 1098 (1991).
[23] J. Noack, Ph.D. thesis, Medical University Lübeck, 1998.
[24] J. Noack and A. Vogel, Appl. Opt. **37** (accepted).
[25] M. H. Rice and J. M. Walsh, J. Chem. Phys. **26**, 824 (1957).
[26] R. T. Knapp, J. W. Daily, and F. G. Hammit, *Cavitation* (McGraw–Hill, New York, 1970).
[27] F. Docchio, P. Regondi, M. R. C. Capon, and J. Mellerio, Appl. Opt. **27**, 3661 (1988).
[28] P. K. Kennedy, IEEE J. Quantum Electron. **31**, 2241 (1995).
[29] R. V. Ambartsumyan, N. G. Basov, V. A. Boiko, V. S. Zuev, O. N. Krokhin, P. G. Kryukov, Y. V. Senat-Skii, and Y. Y. Stoilov, Sov. Phys. JETP **21**, 1061 (1965).
[30] F. Docchio, P. Regondi, M. R. C. Capone, and J. Mellerio, Appl. Opt. **27**, 3669 (1988).
[31] J. H. Marburger, in *Progress in Quantum. Electronics* (Pergamon, Oxford, 1975), Vol. 4, pp. 35–110.
[32] W. L. Smith, P. Liu, and N. Bloembergen, Phys. Rev. A **15**, 2396 (1977).
[33] Q. Feng, J. V. Moloney, A. C. Newell, E. M. Wright, K. Cook, P. K. Kennedy, D. X. Hammer, B. A. Rockwell, and C. R. Thompson, IEEE J. Quantum Electron. **QE-33**, 127 (1997).
[34] J. Lighthill, *Waves in Fluids* (Cambridge University Press, Cambridge, 1978).
[35] R. H. Cole, *Underwater Explosions* (Princeton University Press, Princeton, NJ, 1948).
[36] A. G. Doukas, A. D. Zweig, J. K. Frisoli, R. Birngruber, and T. F. Deutsch, Appl. Phys. B: Photophys. Laser Chem. **53**, 237 (1991).
[37] A. Vogel and W. Lauterborn, J. Acoust. Soc. Am. **84**, 719 (1988).
[38] A. Brodeur, C. Y. Chien, F. A. Ilkov, S. L. Chin, O. G. Kosareva, and V. P. Kandidov, Opt. Lett. **22**, 304 (1997).
[39] O. G. Kosareva, V. P. Kandidov, A. Brodeur, C. Y. Chien, F. A. Ilkov, and S. L. Chin, Opt. Lett. **22**, 1332 (1997).
[40] T. Juhasz, G. Kastis, C. Súarez, T. Turi, Z. Bor, and W. E. Bron, in *Laser Tissue Interaction VII*, Proc. SPIE edited by S. L. Jacques (SPIE, Bellingham, WA, 1996), Vol. **2681, pp.** 428–436.
[41] K. Jungnickel and A. Vogel, Lasers and Light in Ophthalmol. **5**, 95 (1992).
[42] A. Vogel, T. Günther, M. Asiyo-Vogel, and R. Birngruber, J. Cataract. Refractive Surg. **23**, 1301 (1998).